Hindawi
Advances in Materials Science and Engineering
Volume 2021, Article ID 7548071, 16 pages
https://doi.org/10.1155/2021/7548071

Research Article

Investigation on Numerical Simulation of Chloride Transport in Unsaturated Concrete

Qingzhang Zhang,[1,2] **Feng Wang**,[1] **Yifeng Ling**,[3] **Hui Chen**,[4] **and Zhongyuan Li**[1]

[1]*College of Civil Engineering, Henan University of Technology, Zhengzhou 450001, China*
[2]*Key Laboratory of Performance Evolution and Control for Engineering Structures of Ministry of Education, Tongji University, Shanghai 200092, China*
[3]*School of Qilu Transportation, Shandong University, Jinan 250002, China*
[4]*Department of Architecture and Civil Engineering, Wenzhou Institute of Technology, Wenzhou 325035, China*

Correspondence should be addressed to Yifeng Ling; rogeryyy@163.com

Received 14 May 2021; Revised 26 July 2021; Accepted 21 October 2021; Published 17 November 2021

Academic Editor: Luís Evangelista

Marine atmosphere environment accelerates the process of chloride penetration into concrete under the coupling effect of ambient temperature and relative humidity, thereby reducing the durability and service life of concrete. This paper aims to investigate the change of water equilibrium saturation and the chloride transport properties of concrete materials in different environments. The water equilibrium saturation tests at three temperatures and five relative humidity (RH) and salt spray erosion tests at three temperatures were performed. The influence of RH and temperature on the equilibrium saturation of concrete and the influence of temperature and time on the chloride diffusion coefficient are investigated. The results show that, in the process of moisture absorption and desorption, the equilibrium saturation of concrete gradually decreases as temperature rises. At the same depth of concrete, the chloride content gradually increases with temperature increasing, as well as the chloride diffusion coefficient. However, as the corrosion time of salt spray increases, the altering of chloride diffusion coefficient becomes less. Based on the Kelvin equation, a relationship between capillary pressure and water saturation in concrete was established, and a moisture transfer model for concrete in the process of moisture absorption and desorption was derived. Further, based on the established chloride diffusion equation and heat balance equation, a model of temperature-wet-chloride coupling chloride transfer was derived. Theory model simulation results show the transfer speed of chloride under the coupling of diffusion and capillary is higher than pure diffusion in moisture in the absorption process. However, the opposite is true in the desorption process. Moreover, with the increment of saturation rate, the capillary effect on chloride transport is enhanced.

1. Introduction

Concrete structures in coastal areas are often directly exposed to a high chloride environment during service life. Under the long-term impact of salt spray, the chloride content in concrete reaches the threshold level, which leads to the corrosion of steel bar in concrete structure, and the reduction of safety performance [1–4]. Chloride penetration also causes a decrease in the durability of concrete structures [5–7].

The main driving force of chloride transport in concrete is diffusion and capillary action [8, 9]. In addition, factors such as temperature, RH, surface chloride content, water–cement ratio, and mineral admixtures affect the chloride transport process in concrete [10–12]. The Life-365 calculation program developed by the 365 Committee of the United States put forward the equation of the relationship between the chloride diffusion coefficient for ordinary Portland cement concrete and the water–cement ratio [13]. The study performed by Zhang et al. [14] confirmed that RH played an important role in the chloride diffusion coefficient; that is, the chloride diffusion coefficient increased with RH increasing. Zhu et al. [15] explored the effect of environmental RH on the permeability of chloride in unsaturated

concrete. The results showed that when RH was greater than 75%, the content of chloride in concrete increased gradually, while the content of chloride on the surface decreased gradually over time. Shen et al. [16] further researched and found that a higher RH accelerated the migration of chloride in the concrete. Qi et al. [17] analyzed the variation of chloride diffusion coefficient with temperature using the Nernst–Einstein equation and then established the diffusion coefficient equation in the function of temperature. Matsumura et al. [18] found that the chloride diffusion coefficient became larger with higher temperature, and the logarithm of diffusion coefficient was linearly related to the reciprocal of temperature. Environmental RH influences the process of chloride transport and further impacts the transport rate and corrosion depth of chloride in concrete.

Liu et al. [19] reported that the time of chloride salt erosion and the erosion methods (dry-wet cycle, continuous erosion) affected the chloride diffusion coefficient. Li and Li [20] proposed a chloride transport model in cover concrete under drying-wetting cycles. Chen and Liu [21] found that the water migration rate in the drying stage was much less than the wetting stage. For this, Lin and Jiang [22] considered the water transfer speed in the process of moisture absorption and desorption of concrete and established the water transport equation under the drying-wetting cycle environment by adopting multiple water diffusion coefficients. On the basis of the water transport equation, Lin et al. further put forward the chloride transport equation under the drying-wetting cycle environment. Based on the diffusion of water transport in concrete and the permeation of water, Sun et al. [23] obtained a chloride transport model in unsaturated concrete and found that the chloride content in concrete was independent of the dry–wet ratio. Sun et al. [24] studied the effects of water–cement ratio, NaCl solution concentration, and exposure time on chloride diffusion coefficient, penetration depth, and content in concrete under dry-wet circulation.

From the above literature, it can be concluded that the moisture transport rate of concrete during moisture absorption and desorption processes is not consistent with RH. The fact is that chloride diffusion and capillary are very dependent on environmental temperature and humidity. However, the effects of concrete capillarity on chloride transport in different temperatures and RHs have rarely been investigated. Thus, it is necessary to establish a chloride transport model to express the influence of temperature and humidity in different moisture absorption and desorption environments so that the mechanism of unsaturated chloride transport could be better demonstrated.

Therefore, this study investigated the influence of RH and temperature on capillary pressure in water transport using concrete moisture absorption and desorption tests and then determined the parameters of the water transport model. The variation of chloride diffusion coefficient with temperatures and time was evaluated by the chloride penetration test. A chloride transport equation was established in function of capillary action and diffusion. Further, the effects of saturation on chloride transport were simulated by the numerical model.

2. Experimental Program

2.1. Test Materials. The concrete specimens were made of cement, mineral powder, fine aggregate, and coarse aggregate. The binder material comprised P.O. 42.5 cement and mineral powder with densities of 3060 kg/m^3 and 2890 kg/m^3, respectively, in equal mass fractions. The chemical compositions of cement and mineral powder are shown in Table 1. Fine aggregate is well-graded medium sand with a practical density of 2623 kg/m^3 (Table 2). Coarse aggregate is 5~20 mm continuous graded gravel with a maximum particle size of 20 mm (Table 3). Its practical apparent density is 2710 kg/m^3.

The mix proportion of concrete in the chloride diffusion test is shown in Table 4. The W-2 mix proportion concrete mixture ratio of the moisture absorption and desorption equilibrium test is the same as that in Table 4. The concrete specimens in the dimension of 100 mm × 100 mm × 100 mm were prepared and cured at 20 ± 2°C and 95% RH for 28 days. At the age of 28 days, the compressive strength of cubic concrete specimens with the size of 150 mm was measured as shown in Table 4.

2.2. Moisture Absorption and Desorption Test. A total of 40 specimens were cut horizontally into three pieces in the dimension of 100 mm × 100 mm × 30 mm. To avoid the test error, the middle piece was selected to test.

The test was carried out in accordance with ISO12571-2013 standard [25]. In the moisture absorption test, the specimens were first dried at 100°C for 24 hours. After the specimens were cooled to 20°C, they were weighed and recorded. Then, the specimens were dried for 12 h and weighed again until the mass loss was less than 0.5%. In the moisture desorption test, the dry specimens obtained according to the above test method were firstly soaked in water for 7 days to be saturated. Second, the surface of specimens was dried by towels and their weights were measured. The above two procedures were repeated until the weight loss was less than 0.5% in 24 hours to ensure a saturated specimen.

As seen in Figure 1(a), the middle part of the glass container is a porous ceramic partition. During the experiment, the testing specimen was placed on the ceramic partition. The temperature and RH under each test condition were monitored by a thermohygrometer in real time. Any change would be adjusted in time. The glass container was placed in a constant temperature and RH chamber (Figure 1(b)), with ±1°C and ±2.0% precision in temperature and RH, respectively. The designated RHs of 10%, 35%, 80%, and 95% in the glass container were controlled by LiCl, $MgCl_2$, KBr, and KNO_3 saturated salt solutions, respectively. The 50% RH was directly controlled by the chamber. The test was carried out at the temperatures of 20°C, 35°C, and 50°C.

Hereafter, the specimens for moisture absorption and desorption test were put into glass containers which were moved to a constant temperature/humidity chamber. Isothermal absorption devices are shown in Figure 1(b). Then, the mass of each specimen was measured periodically until

Table 1: Chemical compositions of cement and mineral powder in mass (%).

Composition	SiO_2	Fe_2O_3	Al_2O_3	CaO	MgO	Na_2O	SO_3
Cement	22.4	3.7	4.7	60.3	2.7	0.13	2.1
Mineral powder	34.8	1.21	14.32	35.58	11.32	0.14	1.54

Table 2: Particle size distribution of fine aggregate.

Size of screen mesh (mm)	4.75	2.36	1.18	0.60	0.30	0.15
Passing percent (%)	99.5	87.7	72.0	45.9	19.6	2.1

Table 3: Particle size distribution of coarse aggregate.

Size of screen mesh (mm)	26.5	16	9.5	4.75	2.36
Passing percent (%)	100.0	76.0	14.4	0.3	0.0

Table 4: Mix proportion of concrete.

Number	W/B	Water kg/m^3	Binder material kg/m^3	Fine aggregate kg/m^3	Coarse aggregate kg/m^3	Compressive strength (28 d) MPa
W-1	0.36	233	645	514	960	38.9
W-2	0.46	261	562	514	960	35.2
W-3	0.56	282	499	514	960	26.1
W-4	0.66	299	448	514	960	24.2

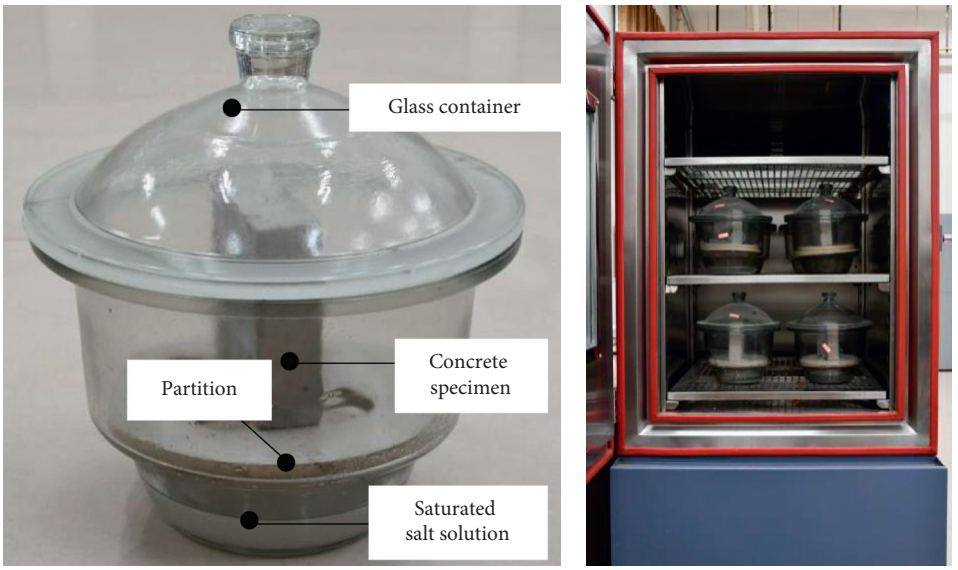

(a) (b)

Figure 1: Isothermal absorption devices: (a) glass container and (b) constant temperature/humidity chamber.

the change in mass was less than 0.1%. Due to high moisture absorption (desorption) in the early stage, the corresponding time interval of measurement was small while it was large in the late stage. There were 12 weight measurements for the absorption test and 13 weight measurements for the desorption test. The measurement results showed that, in the moisture absorption environment of different temperatures, the concrete specimens need 325 h and 100 h to reach equilibrium for RH >50% and RH <50%, respectively. In the moisture desorption environment of different temperatures, the equilibrium time was 150 h and 200 h for RH >50% and RH <50%, respectively.

For porous cement-based materials, moisture saturation can be used as a function of moisture content changes in mass [26]. The equilibrium saturation of concrete in different environments can be described as follows [27]:

$$S = \frac{m_w - m_d}{m_{ws} - m_d}, \quad (1)$$

where S is the mass of specimen underwater (kg), m_w is the mass of specimen underwater (kg), m_d is the mass of specimen in a dry state (kg), and m_{ws} is the mass of specimen under saturation state (kg).

2.3. Chloride Transport Test. To better reflect the impact of environmental parameters on the chloride penetration in concrete, five surfaces of each specimen were smeared with epoxy resin to only allow chloride to penetrate from the other side.

Then, the specimens were placed in a salt spray box to simulate the chloride penetration environment by controlling the salt spray concentration and temperature. In the salt spray penetration test, the temperature for the specimens of W-1 to W-4 was 35°C. As a reference, temperatures of 20°C and 50°C were also used for W-2 specimens. The saltwater concentration in salt spray box was 50 g/L, and the test period was 60 days. The average of 4 specimens for each mix was reported.

The powder for chloride content test was drilled from the specimens every 20 days. After dried and weighted, the powder sample was put in deionized water and stirred evenly. The chloride content was measured by a rapid determination instrument.

3. Results and Discussion

3.1. The Equilibrium Relationship between RH and Saturation. In the moisture absorption and desorption tests, the mass change rate of concrete is the equilibrium saturation under corresponding environment conditions when it reaches the equilibrium state. The equilibrium saturation of moisture absorption and desorption tests at 20°C, 35°C, and 50°C were calculated by equation (1). The equilibrium curves of RH and saturation in moisture absorption and desorption tests at different temperatures are shown in Figure 2.

In Figure 2(a), it can be seen that the trend of the equilibrium saturation curve is similar under three temperatures for absorption. Specifically, for a given temperature, the equilibrium saturation increases with the increment of RH. Moreover, regardless of RH, the equilibrium saturation of concrete gradually decreases as the temperature increases. The relationship between RH and maximum pore size can be determined by the Kelvin equation [28]. The maximum pore size that can be saturated is about 4 nm when RH is 50%. Generally, the boundary between gel pore and capillary pore is 10 nm (i.e., gel pores <10 nm, capillary pores >10 nm). Therefore, when RH is less than 50%, only a few gel pores are saturated, while RH >50%, the capillary pores are gradually saturated [29]. It indicates that RH is dominant for equilibrium saturation of concrete when it is higher than 50%. When RH is below 50%, the temperature impact is not significant on saturation. When RH >50%, the saturation increases most at 20°C, and least at 50°C. It also shows that the effect of temperature on moisture absorption became considerable.

As seen in Figure 2(b), the trends of desorption are similar. For a given temperature, saturation decreases with RH decreasing. At 50°C, the trend is almost linear. Despite the same RH, the equilibrium saturation gradually decreases with the increase in temperature. It is found that the variation of saturation is limited when RH >80%. However, when RH <80%, saturation greatly decreases. It indicates that 80% RH is an inflection point for saturation in desorption.

It can be seen from Figure 2 that, under the same RH, the desorption curve with higher saturation has an obvious hysteresis compared with the absorption process. The main reason for the hysteresis is the "ink bottle effect," which reflects the effects of micropores (bottleneck) connected with the macropores (bottle body) on the flow of water in and out [30]. It is apparent that RH required for the macropores to reach saturation is higher than that for the micropores. For the initially saturated pores, when RH is gradually reduced, the liquid water in the large pores has to transfer through the small pores and could not form a gas-liquid interface by itself. Hence, only when RH drops below the saturated RH in micropores, the water in the macropores could be discharged.

In the processes of moisture absorption and desorption, saturation is an important parameter to ascertain the water content of concrete. To represent the equilibrium relationship between RH and saturation in concrete, an absorption model of porous hygroscopic material between water absorption capacity and RH was adopted in [31]:

$$W = \left[\frac{-\ln(1-h)}{A(T-B)}\right]^{1/c}, \quad (2)$$

where W is the equilibrium moisture content; h is RH; T is temperature (K); and A, B, and C are coefficients.

The saturation of equilibrium moisture content was used instead of the equilibrium moisture content in equation (2), and equation (2) was turned into an inverse function; the relationship model between RH and saturation is acquired as

$$h = \exp\left(-A(T+B)S^C\right), \quad (3)$$

where S is the saturation.

According to Figure 2, parameters A, B, and C in equation (3) can be determined by nonlinear regression. The models of RH and equilibrium saturation in moisture absorption and desorption processes are shown as follows:

$$h_{as} = 1 - \exp\left(-0.03(T-180.7)S^{0.837}\right) R^2 = 0.91, \quad (4)$$

$$h_{ds} = 1 - \exp\left(-0.05(T-258.76)S^{5.04}\right) R^2 = 0.91. \quad (5)$$

For unsaturated concrete, capillary pressure is the main driving force for moisture transfer. Consequently, the relationship between capillary pressure and saturation is the key to investigating moisture transport [32, 33]. Such relationship proposed in the literature is as follows [26]:

$$p_c = \frac{\rho_1 RT}{M} \ln h, \quad (6)$$

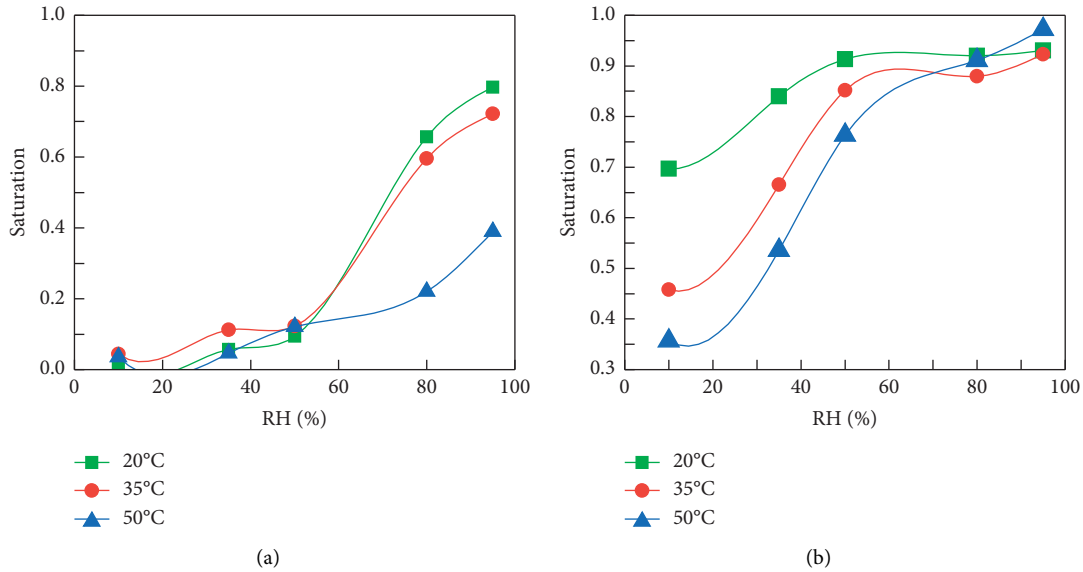

Figure 2: Equilibrium curve of moisture absorption and desorption at 20°C, 35°C, and 50°C: (a) moisture absorption and (b) moisture desorption.

where M is the molar mass of water (kg/mol), R is the gas constant (8.3144 J/mol/K), p_c is capillary pressure (Pa), ρ_l is the density of liquid water (kg/m^3).

Substituting equation (6) with equations (4) and (5), the relationship between capillary pressure and saturation parameter during moisture absorption and desorption can be described as follows:

$$p_{as} = \frac{\rho_l RT}{M} \ln\left(1 - \exp\left(-0.03\,(T - 180.7)S^{0.837}\right)\right), \quad (7)$$

$$p_{ds} = \frac{\rho_l RT}{M} \ln\left(1 - \exp\left(-0.05\,(T - 258.76)S^{5.04}\right)\right). \quad (8)$$

Compared with saturated concrete, the pores in unsaturated concrete are not completely transporting fluid, and the permeability coefficient of water in unsaturated concrete is related to the degree of pore saturation. Thus, the relative permeability of moisture in the process of moisture absorption and desorption is relevant to the saturation of concrete. According to [34], relationships between capillary pressure and saturation as well as relative permeability and saturation can be established as

$$p_c = A_a\left(S^{-1/m} - 1\right)^{1-m}, \quad (9)$$

$$k_{rl}(S) = \sqrt{S}\left[1 - \left(1 - S^{1/m}\right)^m\right]^2, \quad (10)$$

where m can be determined by regression of capillary pressure and saturation curve. The relationship between capillary pressure and saturation at different temperatures in moisture absorption and desorption can be given by equation (9). The m values are shown in Table 5.

Afterward, the relationship between the relative permeability and saturation in the moisture absorption and desorption is established as follows:

Table 5: m values corresponding to the absorption and desorption process.

	Absorption			Desorption		
T (K)	293.15	308.15	323.15	293.15	308.15	323.15
m	0.672	0.579	0.573	0.328	0.324	0.362
R^2	0.985	0.988	0.991	0.999	0.997	0.992

$$k_{rl-as}(S) = \sqrt{S}\left[1 - \left(1 - S^{2.89\ln(T)-14.8}\right)^{1/[2.89\ln(T)-14.89]}\right]^2,$$
$$k_{rl-ds}(S) = \sqrt{S}\left[1 - \left(1 - S^{21.06-3.16\ln(T)}\right)^{1/[21.06-3.16\ln(T)]}\right]^2. \quad (11)$$

The m values under different temperatures in moisture absorption and desorption were calculated using equation (9). However, when equation (9) was used to ascertain A_a values according to Table 5, the fitting correlation coefficient was only 0.56. Therefore, it was not appropriate to use m to characterize the relationship between capillary pressure and saturation in equation (9). In absorption and desorption, equations (7) and (8) can be used to describe the relationship between capillary pressure and saturation.

3.2. Effect of Temperature on Chloride Content. The specimen was subjected to a salt spray penetration test. The chloride content at different depths of concrete at 20 days, 40 days, and 60 days under 20°C, 35°C, and 50°C is shown in Figure 3.

Figure 3 shows that the chloride content gradually decreases as the depth increases. The chloride content at different depths and the penetration depth of chloride increases over time. Regardless of time, the chloride content at a given depth in concrete shows the same trend; that is, the chloride content increases with the increase of

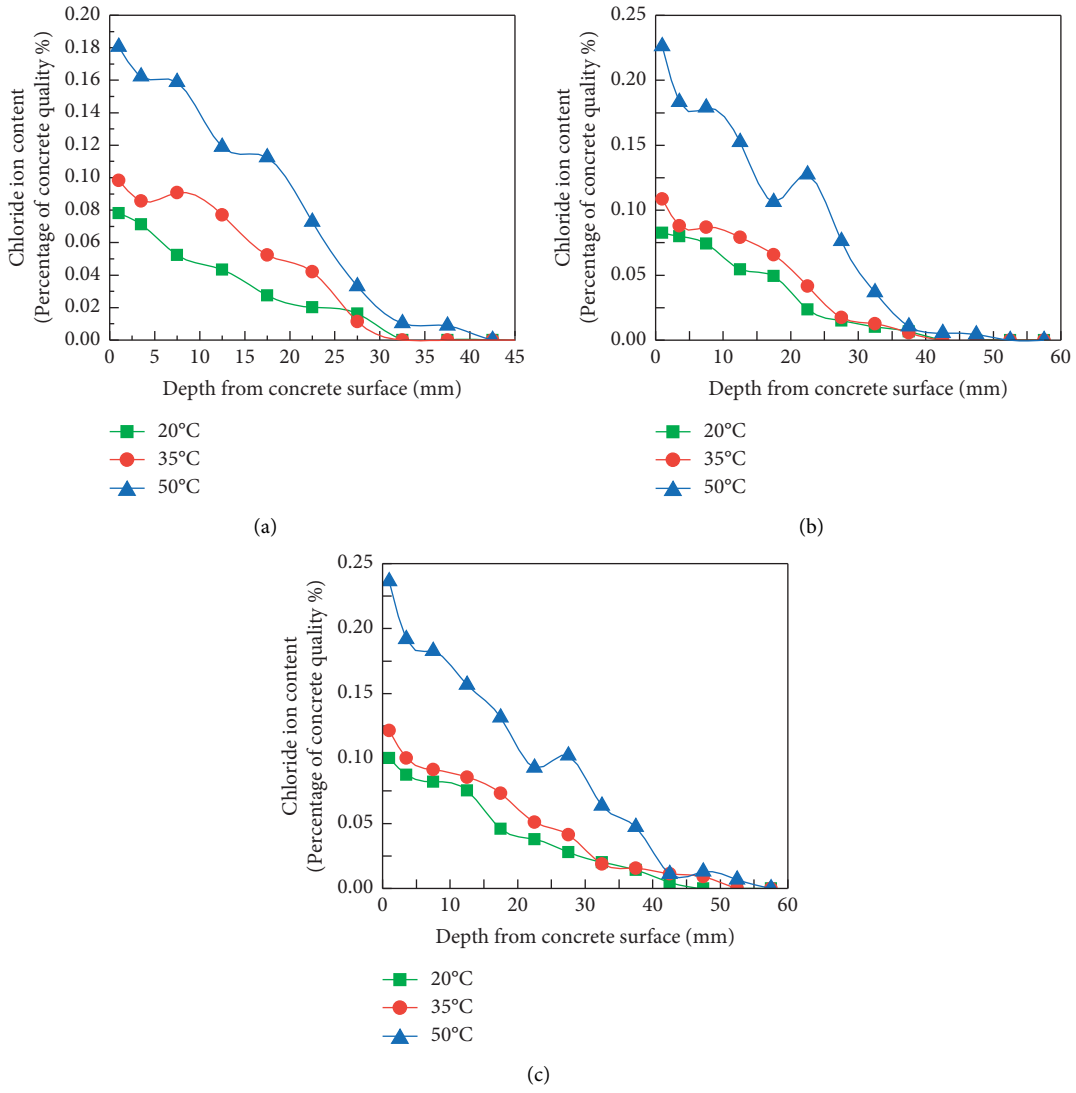

Figure 3: Distribution of chloride content in concrete under different temperatures: (a) 20 d, (b) 40 d, and (c) 60 d.

temperature. It reveals that the increased temperature accelerated chloride penetration and enlarged the penetrated amount of chloride.

3.3. Effect of Temperature on Chloride Diffusion Coefficient. Diffusion is the main driving force for chloride to penetrate saturated concrete. The stable diffusion of chloride can be described by the Fick second law [35]:

$$\frac{\partial C_{Cl}}{\partial t} = D_{Cl}\frac{\partial^2 C_{Cl}}{\partial x^2}, \tag{12}$$

where D_{Cl} is the chloride diffusion coefficient (m^2/s), C_{Cl} is the chloride content (% of the mass of concrete), t is the time (s), and x is the depth from the concrete surface (m).

Assuming that the chloride content on the surface of the concrete structure is constant, D_{Cl} is constant, and the initial chloride content at the exposed surface is 0. The following equation can be derived:

$$C_{Cl} = (C_S - C_0)\left[1 - \operatorname{erf}\left(\frac{x}{2\sqrt{D_{Cl}t}}\right)\right], \tag{13}$$

where C_S is the surface chloride content (% of the mass of concrete) and C_0 is the initial chloride content, which is assumed to be 0.

The test results in Figure 3 were fitted by equation (13) to achieve the chloride diffusion coefficient at different temperatures and penetration times. The chloride diffusion coefficient with different temperatures and penetration time is shown in Figure 4.

Figure 4 shows that the chloride diffusion coefficient gradually increases as the temperature increases, which is consistent with Matsumura's finding [18].

In Figure 4, the chloride diffusion coefficient at 40 d is significantly smaller than that at 20 d, and it is slightly increased compared with that at 60 d. This demonstrates that with temperature rising, its effect on the chloride diffusion coefficient becomes smaller. But in the temperature range

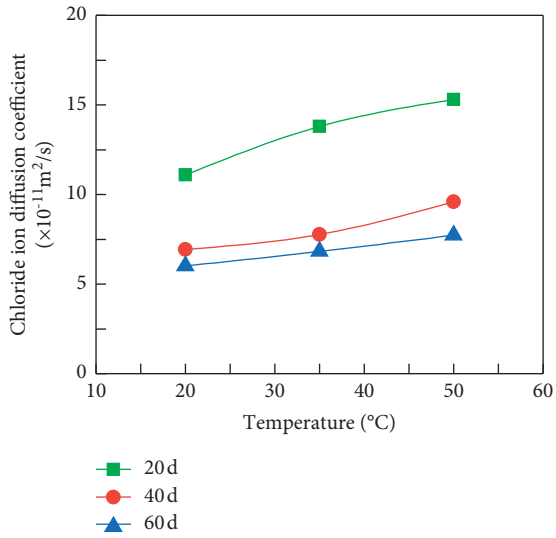

Figure 4: Chloride diffusion coefficient with different temperatures and penetration time.

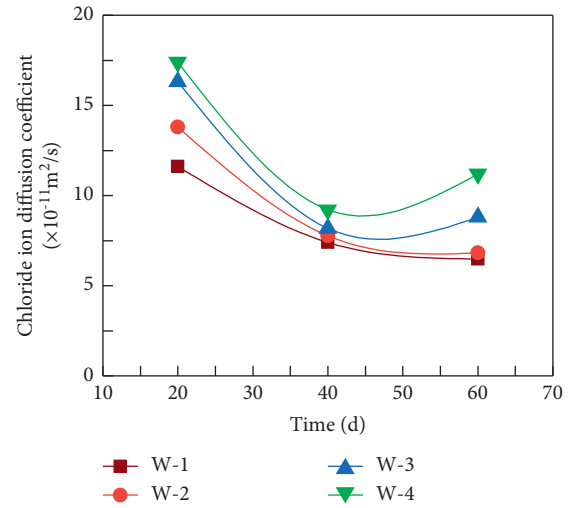

Figure 5: Chloride diffusion coefficient over time.

from 20°C to 50°C, the chloride diffusion coefficient is increased by 37.8%. This is because the higher temperature tends to decrease the resistance of chloride penetration in concrete, which increases the rate of chloride penetration [36]. However, the chloride diffusion coefficient approach to a certain value gradually over time.

There are two models that describe the relationship between chloride diffusion coefficient and temperature. The one reported by Berke is called the Nernst–Einstein equation and the other is proposed in the American Life-365 standard design program. After the dimensionless processing and fitting comparison on the results in Figure 4, it is found that the model proposed in the American Life-365 standard design program is more suitable. The proposed diffusion coefficient model is as follows [37]:

$$D_{Cl} = D_{\text{ref}} \exp\left[\frac{U}{R}\left(\frac{1}{T_{\text{ref}}} - \frac{1}{T}\right)\right], \tag{14}$$

where D_{ref} is the chloride diffusion coefficient corresponding to temperature T_{ref} (m^2/s), U is the activation energy in diffusion (7841 J/mol from the test results), and T_{ref} is the absolute temperature (293.15 K).

3.4. Effect of Time on Chloride Diffusion Coefficient. Figure 5 shows the results of the salt spray test. The chloride diffusion coefficient decreases with time before 40 d. After 40 d, the chloride diffusion coefficient of W-1 and W-2 also decreases, while it increases for W-3 and W-4 with a larger water–cement ratio. The reason may be related to the discrete specimen itself. Overall, the chloride diffusion coefficient decreases over time.

Based on a large number of experimental data, Mangat and Molloy [38] acquired a relationship of the chloride diffusion coefficient in concrete with time as follows:

$$D_{\text{Cl}} = D_1\left(\frac{t_1}{t}\right)^{\alpha}, \tag{15}$$

where t_1 is reference time, that is, exposure time of the first sample (s), t is exposure time greater than the reference time (s), D_1 is the chloride diffusion coefficient (m^2/s) at t_1, and α is the empirical coefficient.

Figure 5 shows the chloride diffusion coefficient over time. Assuming that t_1 is 20 d, the relative ratio of the chloride diffusion coefficient is averaged under three temperatures for 20 d, 40 d, and 60 d. Equation (15) was fitted to determine the empirical coefficient α of 0.65.

4. Chloride Transport Model

4.1. Moisture Transport Model. The main driving force for moisture transport in unsaturated concrete is capillary pressure. In [39], the relationship between the moisture transport velocity and capillary pressure is expressed by the Darcy–Buckingham equation as follows:

$$v = -\frac{k_1}{\mu}\text{grad}\,(p_c), \tag{16}$$

where v is the moisture transfer rate (m/s), k_1 is the effective transport permeability of water (m^2), which is related to the content of water in concrete and the microscopic geometric parameters of the pore, and μ is the dynamic viscosity coefficient of water (Pa·s).

The mass of water flowing into the concrete is equal to the mass flowing out. Regardless of the moisture from liquid to vapor in the pores, the water transport equation can be expressed as [40, 41]

$$v = -\frac{k}{\mu}k_{rl}\frac{\partial p_c}{\partial S}\text{grad}\,(S). \tag{17}$$

The effective permeability of moisture transport can be expressed as

$$k_1 = kk_{rl}, \tag{18}$$

where k is the intrinsic permeability of concrete (m^2) and k_{rl} is the relative permeability, which is a parameter associated with the saturation.

From equations (17) and (18), the moisture transport model in concrete can be described:

$$\frac{\partial \phi\, S}{\partial t} = \operatorname{div}[D(S)\operatorname{grad}(S)], \tag{19}$$

$$D(S) = \frac{k}{\mu} k_{rl} \frac{\partial p_c}{\partial S}, \tag{20}$$

where ϕ is the porosity of concrete and D (S) is the transmission coefficient of liquid water.

The relationship between the dynamic viscosity coefficient of water μ and temperature T can be expressed as follows [42]:

$$\mu = \frac{0.001775}{\left[1 + 0.0837(T - 237.15) + 0.000221(T - 237.15)^2\right]}. \tag{21}$$

Moisture transport consists of absorption and desorption. From equations (19) and (20), two basic parameters can be found: p_c and S. To reflect the real moisture absorption and desorption transport process, the derivatives describing the relationship of capillary pressure and saturation in the process of water absorption and desorption can be obtained according to equations (7) and (8), respectively. Equation (21) was substituted into equation (20) to obtain the moisture transfer coefficient in moisture absorption and desorption, that is, equations (22) and (23):

$$D_{as}(S) = \frac{0.02511 k k_{rl} \rho_1 RT(T - 180.7) S^{-0.163} \exp\left(-0.03(T - 180.7) S^{0.837}\right)}{\mu M\left(1 - \exp\left(-0.03(T - 180.7) S^{0.837}\right)\right)}, \tag{22}$$

$$D_{ds}(S) = \frac{0.252 k k_{rl} \rho_1 RT(T - 258.76) S^{4.04} \exp\left(-0.05(T - 258.76) S^{5.04}\right).}{\mu M\left(1 - \exp\left(-0.05(T - 258.76) S^{5.04}\right)\right)} \tag{23}$$

4.2. Chloride Transport Model. The chloride transport in concrete is essentially a coupling interaction of capillary chloride migration in water and chloride diffusion against concentration difference [22, 43]. The chloride transport flux caused by capillary action is

$$J_{w,c} = C_w \nu, \tag{24}$$

where $J_{w,c}$ is the chloride transport flux caused by capillary action ($kg/(m^2 \cdot s)$) and C_w is the concentration of chloride in pore solution (kg/m^3).

Meanwhile, the relationship between chloride concentration in the pore solution of concrete and free chloride content (percentage of concrete quality) is as follows:

$$C_w = \frac{C_f \rho}{\phi S}. \tag{25}$$

By substituting equations (17) and (25) into equation (24), the chloride transport flux caused by capillary action can be expressed as

$$J_{w,c} = -\frac{C_f \rho}{\phi S} D(S)\operatorname{grad}(S), \tag{26}$$

where C_f is the chloride content in concrete (%) and ρ is the density of concrete (kg/m^3).

The chloride diffusion transport flux caused by chloride content gradient in concrete can be expressed as

$$J_{d,c} = -D_{Cl} \operatorname{grad}\left(C_f\right), \tag{27}$$

where $J_{d,c}$ is the chloride transport flux caused by diffusion.

In concrete pore solution, ions can only be transported by diffusion behavior, which is closely relevant to concrete saturation. Therefore, the chloride diffusion coefficient is largely relevant to the saturation of concrete. Climent et al. found a linear relationship between chloride diffusion coefficient and saturation in unsaturated concrete [44]. Guimarães et al. [45] also put forward the polynomial model, but when the concrete saturation is less than 50%, the reliability of the chloride diffusion coefficient calculated by this model will be reduced. The concrete saturation range established in the water transport model in this paper is large, so the linear model proposed by Climent is used:

$$D_{\mathrm{Cl}}(S) = D_{\mathrm{Cl}} S, \tag{28}$$

where $D_{\mathrm{Cl}}(S)$ is the chloride diffusion coefficient in unsaturated concrete.

Combining equations (14), (15), and (28), the equation of chloride diffusion coefficient in unsaturated concrete can be established:

$$D_{\mathrm{Cl}} = D_1 \exp\left(\frac{U}{R}\left(\frac{1}{T_1} - \frac{1}{T}\right)\right)\left(\frac{t_1}{t}\right)^{\alpha} S. \tag{29}$$

When chloride penetrates the interior of concrete, some ions will be chemically bound by the hydration products in cement to produce new hydrates, and some will be physically adsorbed by the pore surface of interior concrete. The binding capacity of chloride is mainly affected by the content of C_3A in concrete, auxiliary cementitious materials, and PH value of pore solution. Therefore, the total chloride content in concrete is the sum of free chloride content and bound chloride content, which is expressed as follows:

$$C_t = C_b + C_f, \tag{30}$$

where C_b is the bound chloride content in concrete (%).

For chloride transport in concrete, it is necessary to quantitatively express the relationship between the free chloride content and the bound chloride content. Tuutti [46] found that linear binding could well describe such a relationship as follows:

$$C_b = \beta C_f, \tag{31}$$

where β is a constant based on the cementing material and β is 0.15 according to a number of practical engineering surveys in [26].

The chloride transport in concrete is governed by chloride diffusion and moisture capillary and caused by chloride concentration gradient, water flow, and binding interaction. Thus, it can be expressed as

$$\begin{cases} \dfrac{\partial \phi\ S}{\partial t} = \operatorname{div}[D(S)\operatorname{grad}(S)], & (a), \\ \dfrac{\partial C_f}{\partial t} = \operatorname{div}\left[D_{Cl}\operatorname{grad}\left(C_f\right) + \dfrac{C_f D(S)\operatorname{grad}(S)}{\phi S R_K}\right], & (b), \end{cases} \tag{32}$$

where $R_K = (1 + \kappa)$, $\kappa = 0.15$.

4.3. Heat Balance Equation. The heat balance equation correlated to the saturation can be established based on Fourier's law [47] as

$$c\rho\frac{\partial T}{\partial t} + \operatorname{grad}\left(-\lambda_S \operatorname{grad}(T)\right) = Q, \tag{33}$$

where c is the specific heat of the material (J/kg·K), λ_S is the thermal conductivity at different saturations (W/m·K), and Q is the heat flux (J/m^2·s). The negative sign indicates that the direction of heat flow is opposite to the direction of the temperature gradient.

In this paper, the transient plane source (TPS) technique was used to determine the thermal conductivity of concrete for a given mix proportion at the same saturation values of 0, 0.3, 0.5, 0.7, 0.9, and 1.0 in the moisture absorption and desorption. The relationship between the thermal conductivity and saturation is

$$\lambda_S = \left(1 + 0.3432S^2\right)\lambda_a, \tag{34}$$

where λ_a is the thermal conductivity under dry condition (W/m·K).

5. Numerical Simulation

5.1. Model Parameters and Mesh Generation. The concrete is considered as a homogeneous and isotropic continuous medium. The solid skeleton of concrete is assumed as a rigid and invariant material which does not react with liquid phase and gas phase. Based on this assumption, the one-dimensional chloride transport in concrete was explored.

According to equations (22), (23), (29), (32), and (33), a numerical transmission model was established by COMSOL® software. The physical parameters of heat transport are shown in Table 6. The physical parameters of the moisture transport model and the chloride transport model are shown in Table 7.

The size of the moisture transport model is the same as that of the experimental specimen used in the test, namely, 30 mm × 100 mm × 100 mm. A total of 9520 tetrahedral elements were used to develop the finite element model with DOFs (degree of freedom) of 28,186 and convergence criteria of 10^{-5}, as shown in Figure 6(a). Water can only be transmitted through the left boundary with the remaining surfaces closed, and there is no water transmission flux.

The chloride transport model is a two-dimensional geometric model in size of 100 mm × 100 mm. The quadrilateral element is selected for the mesh division of this model. To make the solution domain of model denser, the quadrilateral element is divided by the detailed element size. A total of 578 domain elements and 48 boundary elements were used to develop the finite element model with DOFs of 28,186 and convergence criteria of 10^{-5}, as shown in Figure 6(b). Chloride can only be transmitted through the left boundary, the remaining surfaces are closed, and there is no ion transmission flux.

5.2. Moisture Transport Model Validation. The moisture absorption under three temperatures (20°C, 35°C, and 50°C) and two RH (80% and 90%) conditions was simulated based on the developed model and compared with the corresponding experimental results. The initial saturation and temperature were 0.08 and 283.15k, respectively. The simulation time was the absorption equilibrium time for the three temperatures, which was approximately 350 h. The moisture absorption simulated results and experimental results are shown in Figure 7.

The saturation of concrete increases over time, and its growth rate is similar for different temperatures and RHs, which indicates that the simulated results are in good agreement with the experimental results. However, the experimental values are slightly higher than the simulated values. This is due to the existence of water condensation inside the concrete during the test. Therefore, the moisture absorption in the simulated results is slightly lower than that in the experiment.

The moisture desorption was simulated under temperatures of 20°C, 35°C, and 50°C and RHs of 10% and 35% and compared with the experimental results for validation. The initial saturation of 1 and temperature of 283.15k were used. The boundary saturation of concrete was equilibrium saturation with a simulation time of 250 h.

Figure 8 provides the simulated and experimental results for desorption, which shows good coherence. For 10% RH, the difference between the simulated and the experimental equilibrium saturation increases with temperature increasing. When the concrete is in low saturation, the simulated moisture desorption rate is slightly lower than that of the experiment. It shows that water evaporation has little effect

Table 6: Heat transfer physical parameters.

Parameter	Dry thermal conductivity, λ_a (W/m/K)	Specific heat, c (J/kg·K)	Concrete density, ρ (kg/m^3)	Porosity, ϕ
Value	1.578	900	2297	0.1796

Table 7: Moisture transport and chloride transport physical parameters.

Parameter	Water density, ρ_1 (kg/m^3)	Molar mass of water, M (kg/mol)	Chloride diffusion coefficient, D_l (m^2/s)	Intrinsic permeability, k (m^2)
Value	1000	0.018	1.11×10^{-10}	1.413×10^{-21}

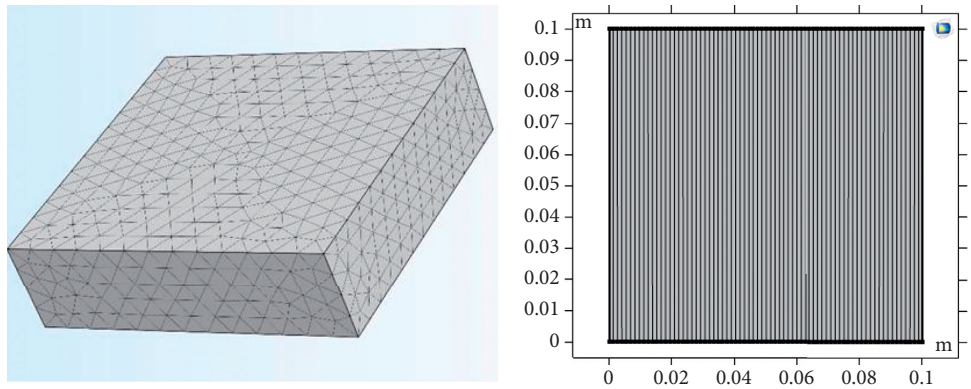

Figure 6: The finite element model of concrete: (a) moisture transport model and (b) chloride transport model.

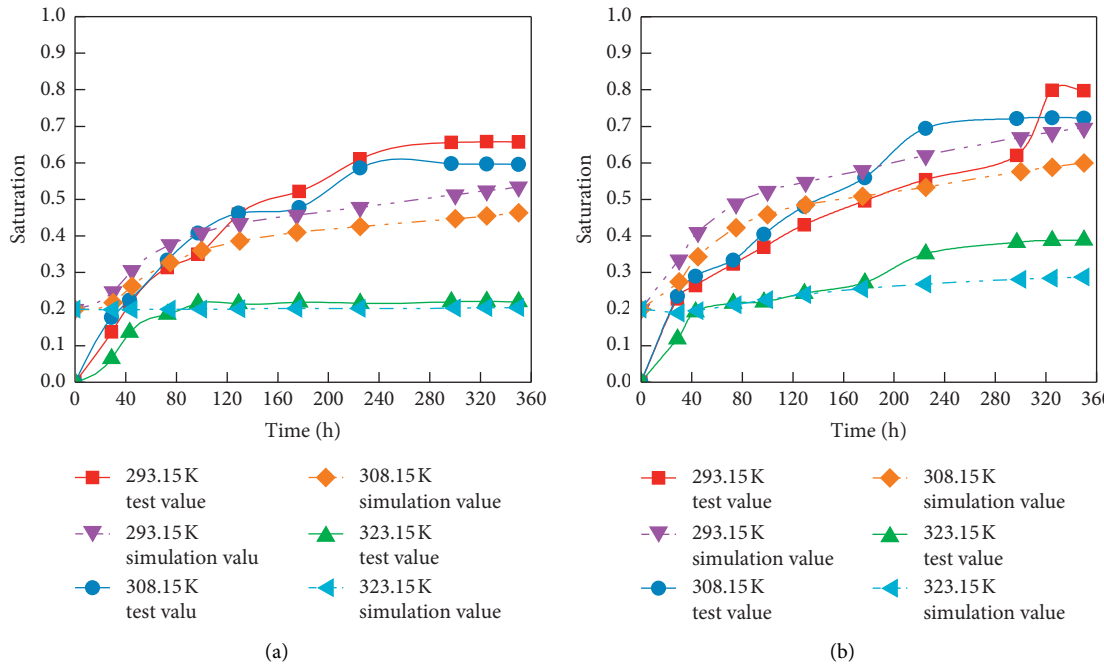

Figure 7: Test and simulation values of moisture absorption process: (a) 80% RH and (b) 95% RH.

on the desorption rate of low saturation concrete, and its effect on equilibrium saturation increases with the increase of temperature. Therefore, the simulated model is accurate.

5.3. Chloride Transport Model Validation in Saturated Concrete. The simulated and experimental results of chloride transport in saturated concrete of 0.46 water–cement

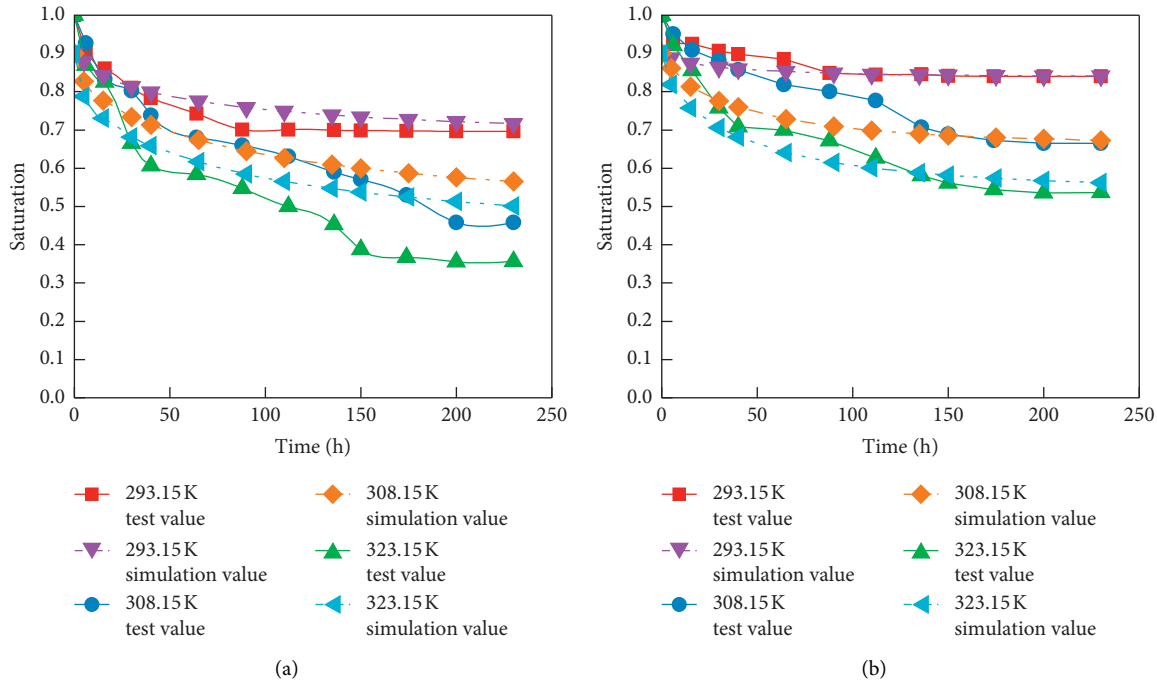

Figure 8: Simulated and experimental results of moisture desorption: (a) 10% RH and (b) 35% RH.

ratio were used for validation. The size of the concrete specimen was 100 mm × 100 mm × 100 mm. The time of chloride penetration test was 60 days. The temperatures of 20°C, 35°C, and 50°C were used with a surface chloride content of 0.105%, 0.123%, and 0.233% as a boundary condition, respectively. The initial temperature was 293.15 K (0°C), and saturation was 1.0. The chloride penetration depth and chloride content distribution under three temperatures at 60 d were simulated.

It can be seen from Figure 9 that the simulated results are basically the same as the experimental results. The simulated chloride penetration depth is greater than that of the experiment. This could be explained as follows: (1) Bao et al.'s [48] study shows that the higher the relative humidity of the specimen-exposed environment leads to the greater water content within the specimen. The chloride diffusion was tested in a closed salt spray corrosion environment with a high RH, resulting in greater internal water content of the concrete specimens. At the same time, the condensation effect of water vapor occurred on the surface of concrete, forming a "water film" to dilute the chloride concentration, resulting in a reduced chloride concentration. Thus, the simulated chloride penetration rate and depth are greater than the experimental values. (2) In the experiment, the chloride content on the concrete surface gradually increased over time, and the results are consistent with the findings in [49], while in simulation, it is larger than the experimental value at 60 d. Therefore, the simulated chloride content is greater than the experimental results.

5.4. Chloride Transport Model Validation in Unsaturated Concrete. Concrete specimens with initial saturation of 0.7 were made with the same proportion as W-2. After curing,

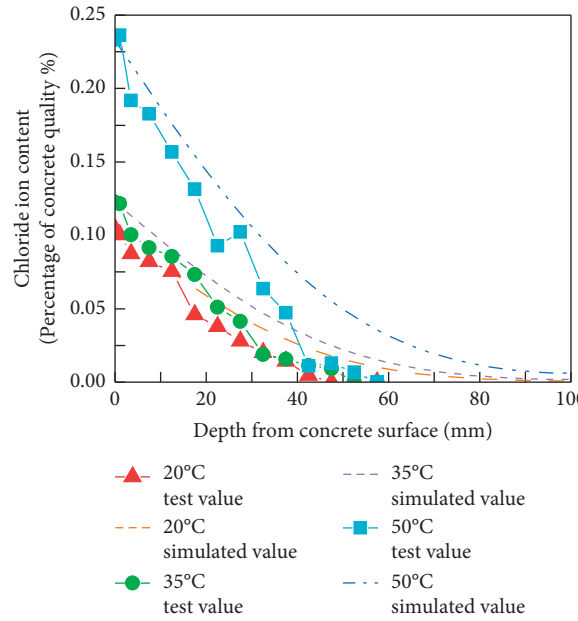

Figure 9: Chloride content distribution in concrete at 20°C, 35°C, and 50°C.

the concrete was cut horizontally into two 100 mm × 100 mm × 50 mm specimens for the chloride penetration test of unsaturated concrete. When the temperature and humidity became equilibrium, 20 g NaCl solid was placed on the top of the specimen. The specimens were wrapped and sealed with plastic film and were then put into a chamber (temperature = 25°C, RH = 50%). The chloride content in concrete was measured by a CLU-S type chloride content tester at 20 and 80 days.

Next, the simulated and experimental results of 0.7 concrete specimens were compared to validate the chloride transport model for unsaturated concrete. The boundary condition ($x = 0$) of chloride content is the experimental value of surface chloride content of 20 d and 80 d, which are 0.0344% and 0.0392%, respectively. Furthermore, the initial saturation of 0.7, the initial temperature of 293.15 K (20°C), and the chloride content of 0 were used for modeling. The comparison result is shown in Figure 10.

According to Figure 10, the trends of simulation coincide with that of the experiment, which effectively proves the reliability of the chloride transport model for unsaturated concrete. The chloride penetration depth was 12 mm and 20 mm at 20 d and 80 d, respectively. The experimental results were slightly smaller than the simulated results.

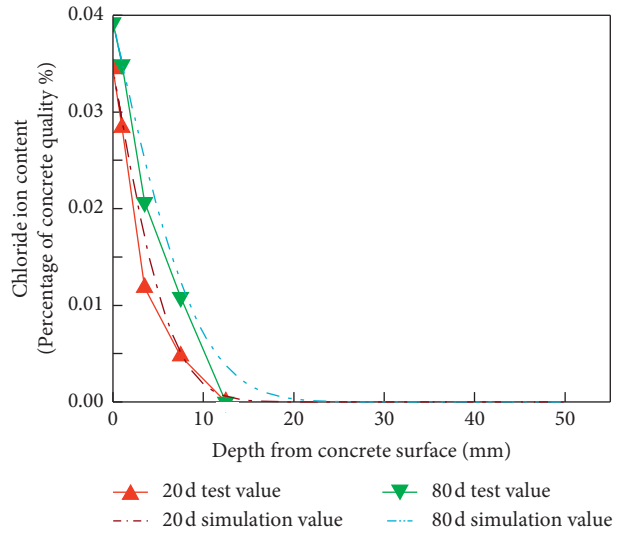

Figure 10: Chloride content distribution in concrete at 20 d and 80 d.

5.5. Capillary Effect on Chloride Transport in Moisture Absorption. The chloride transport in concrete with different saturation under moisture absorption was simulated to evaluate the effects of diffusion and capillary action on chloride transport.

The concrete boundary conditions ($x = 0$) were set as follows: the temperature of the left terminal face of concrete = 308.15 K (35°C); the chloride content = 0.29%; and the saturation = 0.6, 0.8, and 1. The initial condition is as follows: temperature = 293.15 K (20°C), chloride content = 0, and saturation = 0.4. The simulation was calculated with the step length of 1 d and the total duration of 365 d. The distribution of chloride content at 50 mm depth under diffusion is shown in Figure 11, where PDS is pure diffusion saturation and CMAS is coupled moisture absorption saturation.

The chloride content in the boundary conditions of the numerical simulation was based on the experiments, but it is not exactly the same as experiment results. It should be noted that the boundary chloride content (0.2%) at 293.15 K (20°C) was artificially set, which means that the influence of boundary chloride content on chloride transmission was studied. However, the boundary chloride content of 308.15 K (35°C) was calculated according to equation (35). Equation (35) ignores the influence of time on the surface chloride content as seen in Figure 3, which is fitted considering the ratio of temperature parameter (T/T_1) and the relative value of the surface chloride content (C_T/C_1) with R^2 of 0.929:

$$\frac{C_T}{C_1} = 0.0002 \exp\left(8.471\left(\frac{T}{T_1}\right)\right), \tag{35}$$

where T_1 is 293.15 K (20°C), C_1 is the surface chloride content corresponding to $T = 293.15$ K (20°C), and C_T is the surface chloride content corresponding to the temperature T.

It can be seen from Figure 11 that, in moisture absorption, the chloride content is higher in the concrete with greater boundary saturation. However, the difference between chloride content under coupling action and diffusion gradually increases because the chloride transport under coupling action was the result of both diffusion effect and capillary action. Therefore, the chloride transport speed under coupling action is greater than that under pure

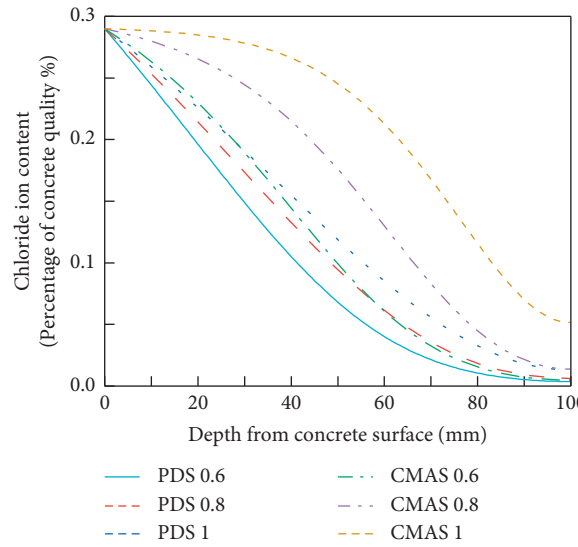

Figure 11: Chloride content distribution under diffusion in moisture absorption.

diffusion. This also indicates that the influence of capillarity action on chloride transport gradually increases with the increment of saturation gradient. When the saturation is 0.6, the effect of capillary action on chloride transport is minimal. At the same time, the difference between the chloride content under the coupling action and pure diffusion increases first and then decreases with the depth increasing. Regardless of saturation, the effect of capillary action on chloride transport increases firstly and then decreases with the increase of depth.

5.6. Capillary Effect on Chloride Transport of Saturation in Moisture Desorption. The chloride transport in concrete with different saturation under moisture desorption was simulated. Comparing the diffusion and coupling transport

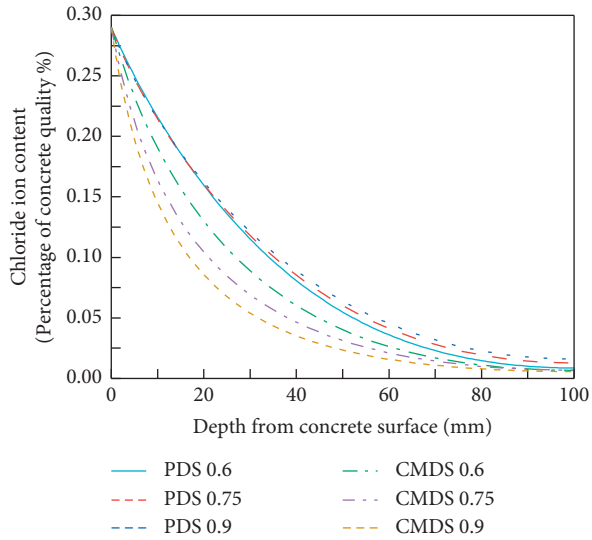

Figure 12: Chloride content distribution under diffusion and coupling action for moisture desorption.

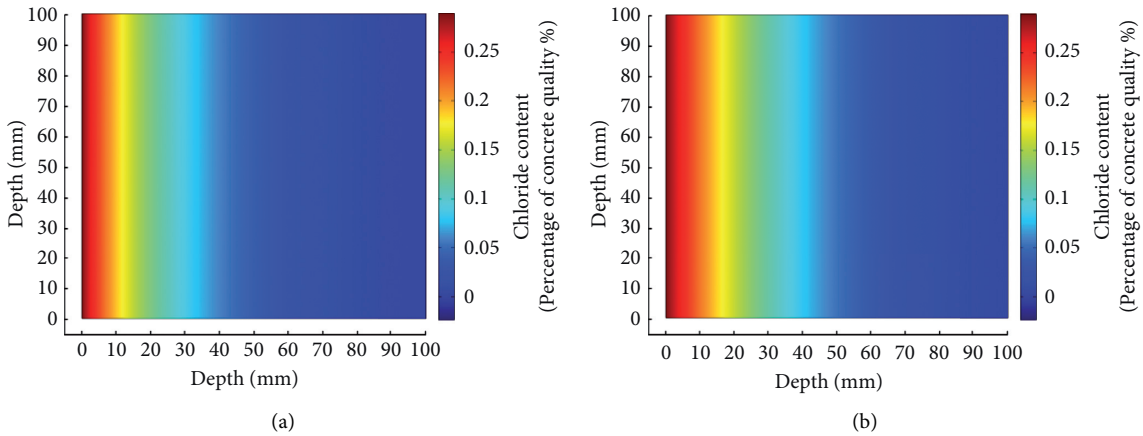

Figure 13: Comparison of chloride coupling migration and pure diffusion in chloride transport model: (a) coupled moisture desorption, saturation 0.6; (b) pure diffusion, saturation 0.6.

(diffusion and capillary action) of chloride in concrete, the influence of coupling transport in the moisture desorption environment was assessed. Furthermore, the effect of capillary action on chloride transport was also investigated.

The concrete boundary conditions ($x = 0$) were set as follows: the temperature of the left terminal face of concrete = 308.15k (35°C), the chloride content = 0.29%, and the saturation = 0.4. The initial condition was as follows: temperature = 293.15 K (20°C); chloride content = 0; and saturation = 0.6, 0.75, 0.9. The simulation was calculated with the step length of 1 d and the total duration of 365 d. The distribution of chloride content at 50 mm in the diffusion and hygrothermal coupling of concrete is shown in Figure 12, where PDS is pure diffusion saturation, CMDS is coupled moisture desorption saturation.

It can be found in Figure 12 that the content of chloride for pure diffusion increased slightly with the increase of saturation while the chloride content decreased gradually with the increase of saturation for coupling action. Meanwhile, with saturation gradient increasing, the difference of chloride content between coupling action and diffusion is increased. The effect of capillary action on chloride transport is gradually enhanced with saturation gradient increasing. When the saturation is 0.9, the difference in chloride distribution between diffusion and coupling action is the largest, and then the effect of capillary action on chloride transport is the strongest. Meanwhile, for a given saturation gradient, the effect of capillary action on chloride transport increases first and then decreases with the increment of depth.

The effect of internal saturation on chloride coupling migration and diffusion transmission is compared in Figures 13–15 at 256 days. It is found that, with the internal saturation increasing, the chloride content at the same depth under the coupling transmission increased while the chloride content at the same depth of pure diffusion transmission is not significant. When the internal saturation was the same, the chloride content of the same depth was larger in pure

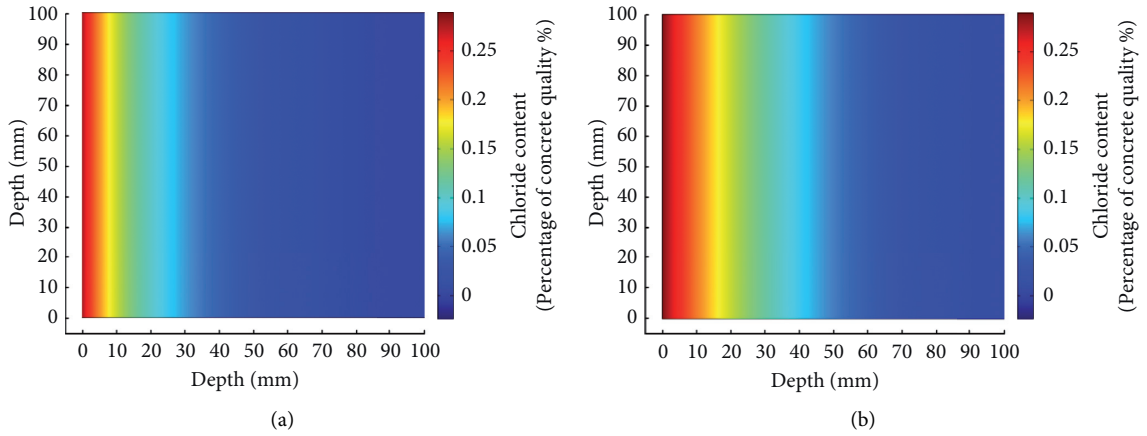

Figure 14: Comparison of chloride coupling migration and pure diffusion in chloride transport model: (a) coupled moisture desorption, saturation 0.75; (b) pure diffusion, saturation 0.75.

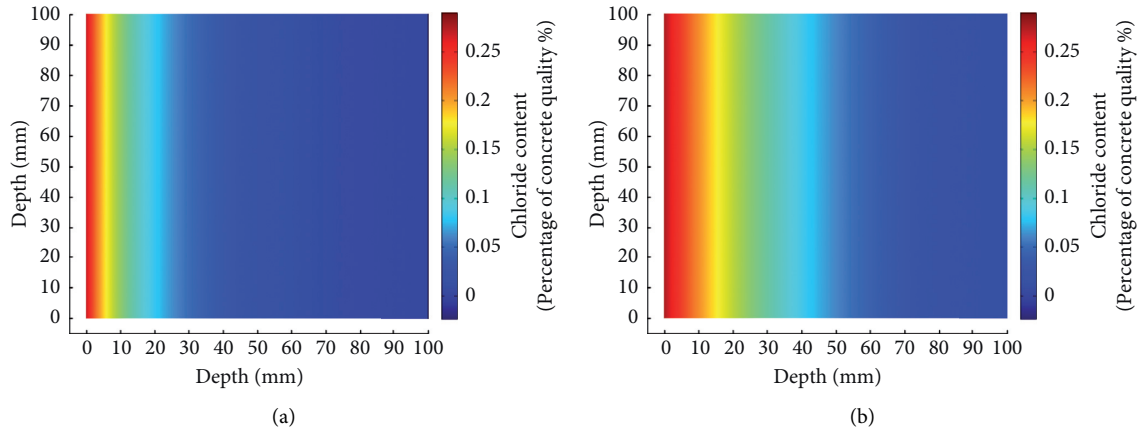

Figure 15: Comparison of chloride coupling migration and pure diffusion in chloride transport model: (a) coupled moisture desorption, saturation 0.9; (b) pure diffusion, saturation 0.9.

diffusion transmission. The reason for this phenomenon is that the effect of the concentration difference under diffusion transmission on the chloride content of the same depth became gradually stabilized, while the effect of capillary action on chloride transmission at the same depth was increasing.

6. Conclusions

In this paper, the diffusion and capillary flux of chloride in unsaturated concrete at different temperatures was experimentally investigated, and the relationship between capillary pressure and concrete saturation at different temperatures was achieved. Further, a transport model of temperature-humidity-chloride was established. The influence of capillary pressure on chloride transport in moisture absorption and desorption was evaluated. From the experimental and simulated results, the following conclusions are drawn:

(1) The inflection points of equilibrium saturation in isothermal moisture absorption and desorption for RH are 50% and 80%, respectively. In the moisture absorption (desorption), when RH is lower than (higher than) the inflection point, the temperature has little effect on the equilibrium saturation. But when RH is higher than (lower than) the inflection point, the saturation increases with temperature decreasing.

(2) The increment of temperature cause the increases in chloride diffusion coefficient, and the increasing rate of chloride diffusion coefficient gradually reduces over time and finally stabilizes.

(3) The simulated model is in good agreement with experimental results. However, it should be pointed out that the chloride transport model of unsaturated concrete has some defects and limitations in the lack of time-varying effect of chloride concentration.

(4) The chloride transport velocity of the coupling environment is higher than that of pure diffusion in a moisture absorption environment with more chloride content found at the same depth. However, the opposite result is presented in the desorption process. Moreover, the effect of capillary action on

chloride transport increased with saturation increasing [50, 51].

Data Availability

The data used to support the findings of this study are included within the article.

Conflicts of Interest

The authors declare that there are no conflicts of interest regarding the publication of this paper.

Acknowledgments

This work was financially supported by the National Natural Science Foundation of China (Grant no. 51509084); the Foundation of Key Laboratory of Performance Evolution and Control for Engineering Structures of Ministry of Education, Tongji University (Grant no. 2018KF-2); the Cultivation Plan for Youth Backbone Teachers of Institution of Higher Education by Henan Province (Grant no. 2019GGJS086); the Fundamental Research Funds for the Henan Provincial Colleges and Universities in Henan University of Technology (Grant no. 2017RCJH03); the Cultivation Plan for Youth Backbone Teachers by Henan University of Technology; and the Innovative Funds Plan of Henan University of Technology (Grant no. 2020ZKCJ05).

References

[1] H. Chang, S. Mu, D. Xie, and P. Wang, "Influence of pore structure and moisture distribution on chloride "maximum phenomenon" in surface layer of specimens exposed to cyclic drying-wetting condition," *Construction and Building Materials*, vol. 131, pp. 16–30, 2017.

[2] J. Z. Zhang, J. Huang, C. Q. Fu, L. Huang, and H. Ye, "Characterization of steel reinforcement corrosion in concrete using 3D laser scanning techniques," *Construction and Building Materials*, vol. 270, Article ID 121402, 2020.

[3] W. Jie, J.-B. M. Dassekpo, C. Wan, and X. Zha, "Experimental and numerical modeling of chloride diffusivity in hardened cement concrete considering the aggregate shapes and exposure-duration effects," *Results in Physics*, vol. 7, pp. 1427–1432, 2017.

[4] C. Fu, D. Fang, H. Ye, L. Huang, and J. Wang, "Bond degradation of non-uniformly corroded steel rebars in concrete," *Engineering Structures*, vol. 226, Article ID 111392, 2021.

[5] S. Guzmán, J. C. Gálvez, and J. M. Sancho, "Cover cracking of reinforced concrete due to rebar corrosion induced by chloride penetration," *Cement and Concrete Research*, vol. 41, no. 8, pp. 893–9902, 2011.

[6] R. B. Murugan, C. Natarajan, and S.-E. Chen, "Material development for a sustainable precast concrete block pavement," *Journal of Traffic and Transportation Engineering*, vol. 3, no. 5, pp. 483–491, 2016.

[7] J. Bao, Z. Yu, and L. Wang, P. Zhang, X. Wan, S. Gao, and T. Zhao, Application of ferronickel slag as fine aggregate in recycled aggregate concrete and the effects on transport properties," *Journal of Cleaner Production*, vol. 304, Article ID 127149, 2021.

[8] L. Song, W. Sun, and J. Gao, "Time dependent chloride diffusion coefficient in concrete," *Journal of Wuhan University of Technology-Materials Science Edition*, vol. 28, no. 2, pp. 314–319, 2013.

[9] N. S. Berke and M. C. Hicks, "Predicting chloride profiles in concrete," *Corrosion*, vol. 50, no. 3, pp. 234–239, 1994.

[10] S. L. Amey, D. A. Johnson, M. A. Miltenberger, and H. Farzam, "Predicting the service life of concrete marine structures: an environmental methodology," *ACI Structure Journal*, vol. 95, no. 1, pp. 27–36, 1998.

[11] L.-x. Mao, Z. Hu, J. Xia et al., "Multi-phase modelling of electrochemical rehabilitation for ASR and chloride affected concrete composites," *Composite Structures*, vol. 207, pp. 176–189, 2020.

[12] C.-l. Zhang, W.-k. Chen, S. Mu, B. Šavija, and Q.-f. Liu, "Numerical investigation of external sulfate attack and its effect on chloride binding and diffusion in concrete," *Construction and Building Materials*, vol. 285, Article ID 122806, 2021.

[13] H. J. Ba, Q. W. Bao, and Z. Y. Chen, *The Standards of the Chinese Society of Civil Engineering. Guide to Durability Design and Construction of Concrete Structures*, China Architecture & Building Press, Beijing, China, 2005.

[14] Y. Zhang, Z. Yang, and G. Ye, "Dependence of unsaturated chloride diffusion on the pore structure in cementitious materials," *Cement and Concrete Research*, vol. 127, Article ID 105919, 2020.

[15] F. Zhu, Z. Ma, and M. Zhang, "Chloride penetration into concrete under the coupling effects of internal and external relative humidity," *Advances in Civil Engineering*, vol. 2020, no. 2, pp. 1–14, 2020.

[16] X.-h. Shen, Q.-f. Liu, Z. Hu et al., "Combine ingress of chloride and carbonation in marine-exposed concrete under unsaturated environment: a numerical study," *Ocean Engineering*, vol. 189, Article ID 106350, 2019.

[17] B. Qi, J. Gao, F. Chen, and D. Shen, "Chloride penetration into recycled aggregate concrete subjected to wetting-drying cycles and flexural loading," *Construction and Building Materials*, vol. 174, pp. 130–137, 2018.

[18] T. Matsumura, K. Shirai, and T. Saegusa, "Verification method for durability of reinforced concrete structures subjected to salt attack under high temperature conditions," *Nuclear Engineering and Design*, vol. 238, no. 5, pp. 1181–1188, 2008.

[19] Q.-f. Liu, M. F. Iqbal, J. Yang, X.-y. Lu, P. Zhang, and M. Rauf, "Prediction of chloride diffusivity in concrete using artificial neural network: modelling and performance evaluation," *Construction and Building Materials*, vol. 268, Article ID 121082, 2021.

[20] C. Q. Li and K. F. Li, "Chlorine transport in dry-wet alternation surface stratum concrete: principle, test and simulation," *Journal of the Chinese Ceramic Society*, vol. 38, no. 4, pp. 22–29, 2010.

[21] W. K. Chen and Q. F. Liu, "Moisture and multi-ions transport in concrete under drying-wetting cycles: a numerical study," *Journal of Hydraulic Engineering*, vol. 52, no. 5, pp. 622–632, 2021.

[22] G. Lin and Y. H. Jiang, "Simulation of chloride transport on coagulation dry-wet alternation," *Journal of Wuhan Polytechnic University*, vol. 28, no. 3, pp. 68–71, 2009.

[23] C. Sun, L. Yuan, X. Zhai, F. Qu, Y. Li, and B. Hou, "Numerical and experimental study of moisture and chloride transport in unsaturated concrete," *Construction and Building Materials*, vol. 189, pp. 1067–1075, 2018.

[24] R. Sun, X. Hu, Y. Ling, Z. Zuo, P. Zhuang, and F. Wang, "Chloride diffusion behavior of engineered cementitious composite under dry-wet cycles," *Construction and Building Materials*, vol. 260, Article ID 119943, 2020.

[25] ISO, *Hygrothermal Performance of Building Materials and Products - Determination of Hygroscopic Sorption Properties: ISO 12571: 2013*, Cen-Cenelec Management Centre, Brussels, Belgium, 2013.

[26] Q. Zeng, Y. Y. Wang, and K. F. Li, "Uniform model for moisture transport in porous materials and its application to concrete at selected Chinese regions," *Journal of Materials in Civil Engineering*, vol. 26, no. 6, pp. 1–8, 2014.

[27] X. Wei, L. Jin, Y. Zhang, and Z. Ding, "Water transport in cracked unsaturated concrete," *Journal of Building Materials*, vol. 2018, no. 21, p. 731, 2018.

[28] Y. Zhang, F. L.-Y. Lam, Z.-F. Yan, and X. Hu, "Review of kelvin's equation and its modification in characterization of mesoporous materials," *Chinese Journal of Chemical Physics*, vol. 19, no. 2, pp. 102–108, 2006.

[29] P. Schiller, M. Wahab, T. Bier, and H.-J. Mögel, "A model for sorption hysteresis in hardened cement paste," *Cement and Concrete Research*, vol. 123, Article ID 105760, 2019.

[30] F. A. L. Dullien, *Porous media: Fluid Transport and Pore Structure*, Academic Press, San Diego, CA, USA, 1992.

[31] C. M. Yu, *Numerical Analysis of Heat and Mass Transfer for Porous Materials*, Tsinghua University Press Beijing, Beijing, China, 2011.

[32] A. Ababneh, F. Benboudjema, and Y. Xi, "Chloride penetration in nonsaturated concrete," *Journal of Materials in Civil Engineering*, vol. 15, no. 2, pp. 183–191, 2003.

[33] P. O'Neill Iqbal and T. Ishida, "Modeling of chloride transport coupled with enhanced moisture conductivity in concrete exposed to marine environment," *Cement and Concrete Research*, vol. 39, no. 4, pp. 329–339, 2009.

[34] M. T. V. Genuchten, "A closed-form equation for predicting the hydraulic conductivity of unsaturated soils," *Soil Science Society of America Journal*, vol. 44, no. 5, pp. 892–898, 1980.

[35] M. Collepardi, A. Marcialis, and R. Turriziani, "Penetration of chloride ions into cement pastes and concretes," *Journal of the American Ceramic Society*, vol. 55, no. 10, pp. 534-535, 1972.

[36] X.-J. Niu, Q.-B. Li, W.-J. Liu, and Y. Hu, "Effects of ambient temperature, relative humidity and wind speed on interlayer properties of dam concrete," *Construction and Building Materials*, vol. 260, Article ID 119791, 2020.

[37] Life-365TM, *Life-365 Service Life Prediction Model TM and Computer Program for Predicting the Service Life and Life-Cycle Costs of Reinforced concrete Exposed to Chlorides*, Silica Fume Association, Freetown, Sierra Leone, 2008.

[38] P. S. Mangat and B. T. Molloy, "Prediction of long term chloride concentration in concrete," *Materials and Structures*, vol. 27, no. 6, pp. 338–346, 1994.

[39] R. Creny and P. Rovnanikova, *Transport Processes in concrete*, CRC Press, London, England, 2002.

[40] V. Baroghel-Bouny, "Water vapour sorption experiments on hardened cementitious materials. Part II: e," *Cement and Concrete Research*, vol. 37, no. 3, pp. 438–454, 2007.

[41] J.-F. o. Daian, "Condensation and isothermal water transfer in cement mortar Part I ? Pore size distribution, equilibrium water condensation and imbibition," *Transport in Porous Media*, vol. 3, no. 6, pp. 563–589, 1988.

[42] Z. S. Ji, R. K. Zhu, and D. Li, *Transmission Principle*, Harbin Institute of Technology Press, Harbin, China, 2017.

[43] E. P. Nielsen and M. R. Geiker, "Chloride diffusion in partially saturated cementitious material," *Cement and Concrete Research*, vol. 33, no. 1, pp. 133–138, 2003.

[44] M. A. Climent, G. de Vera, J. F. López, E. Viqueira, and C. Andrade, "A test method for measuring chloride diffusion coefficients through nonsaturated concrete," *Cement and Concrete Research*, vol. 32, no. 7, pp. 1113–1123, 2002.

[45] A. T. C. Guimarães, M. A. Climent, G. D. Vera, F. J. Vicente, F. T. Rodrigues, and C. Andrade, "Determination of chloride diffusivity through partially saturated Portland cement concrete by a simplified procedure," *Construction and Building Materials*, vol. 25, pp. 785–790, 2011.

[46] K. Tuutti, *Corrosion of Steel in concrete*, Swedish Cement and Concrete Research Institute, Stockholm, Sweden, 1982.

[47] M. Jerman and R. Černý, "Effect of moisture content on heat and moisture transport and storage properties of thermal insulation materials," *Energy and Buildings*, vol. 53, pp. 39–46, 2012.

[48] J. Bao, S. Li, P. Zhang, S. Xue, Y. Cui, and T. Zhao, "Influence of exposure environments and moisture content on water repellency of surface impregnation of cement-based materials," *Journal of Materials Research and Technology*, vol. 9, no. 6, pp. 12115–12125, 2020.

[49] K. Zhao, Y. Qiao, P. Zhang, J. Bao, and Y. Tian, "Experimental and numerical study on chloride transport in cement mortar during drying process," *Construction and Building Materials*, vol. 258, Article ID 119655, 2020.

[50] V. Baroghel-Bouny, M. Mainguy, T. Lassabatere, and O. Coussy, "Characterization and identification of equilibrium and transfer moisture properties for ordinary and high-performance cementitious materials," *Cement and Concrete Research*, vol. 29, no. 8, pp. 1225–1238, 1999.

[51] B. M. Savage and D. J. Janssen, "Soil physics principles validated for use in predicting unsaturated moisture movement in portland cement concrete," *ACI Materials Journal*, vol. 94, no. 1, pp. 63–70, 1997.